Hindawi
Shock and Vibration
Volume 2019, Article ID 8419591, 13 pages
https://doi.org/10.1155/2019/8419591

Research Article

Master-Slave Integrated Control for the Transverse Vibration of a Translational Flexible Manipulator Based on Input Shaping and State Feedback

Jin-yong Ju,[1,2] **Wei Li**,[2] **Yufei Liu**,[1] **and Chunrui Zhang**[3]

[1]*School of Mechanical and Automotive Engineering, Anhui Polytechnic University, Wuhu 241000, China*
[2]*School of Mechatronic Engineering, China University of Mining and Technology, Xuzhou 221116, China*
[3]*Engineering Research and Training Center, Anhui Polytechnic University, Wuhu 241000, China*

Correspondence should be addressed to Yufei Liu; yufeiliucumt@yahoo.com

Received 19 February 2019; Revised 9 April 2019; Accepted 7 May 2019; Published 4 June 2019

Academic Editor: Gabriele Cazzulani

The problem of the elastic vibration control for a translational flexible manipulator system (TFMS) under variable load conditions is studied. The input shaper can effectively filter out the vibration excitation components for the flexible manipulator in the driving signals, but the adaptability and rapidity of the conventional input shaper are poor because it is essentially an open-loop control mode and there are time-lag links inevitably. Thus, by combining the state feedback with the input shaping, a master-slave integrated controller of the TFMS is proposed. Moreover, in order to solve the time-lag effect of the conventional input shaper, based on the optimal algorithm, a two-mode vibration cascade shaper for the TFMS is designed. Then, under variable load conditions, the control effects of the conventional input shapers, the two-mode vibration cascade shaper, and the combination of the state feedback integral controller (SFIC) with the above shapers are investigated. The results show that the designed master-slave integrated controller has high robustness under variable load conditions and takes good account of the requirements of system response time and overshoot for achieving the goal of nonovershoot under fast response speed. Simulation experiment results verify the effectiveness of the designed controller.

1. Introduction

The efficient encapsulation of the integrated circuit (IC) board depends on the precision of the SMT assembly devices. On the SMT assembly line, the packaging equipment is the device whose actuators are mainly assembled by the mechanical manipulator [1, 2]. Thus, the structural and dynamic characteristics of the mechanical manipulator have a very important influence on the encapsulation level of the IC board. The rigid structures are often adopted to the traditional SMT assembly manipulator, and the overall structure is heavy and the structural buffeting is inevitable, which have a great influence on the working efficiency and positioning accuracy of the whole machine. In order to improve the overall performance of the IC packaging machinery, the system structure should be improved to achieve the purpose of lightweight, which is also the basis for high speed and integration. Compared with the rigid manipulator, the flexible manipulator has the advantages of lightweight, high speed, low energy consumption, and so on. However, owing to the low stiffness and large deflection, the flexible manipulator is prone to generate elastic vibration during movement, which is contrary to the requirement of the motion precision for the IC packaging [3, 4]. Thus, it is the precondition for realizing the effective utilization of the flexible manipulator in the packaging equipment to deeply study the system dynamic characteristics and vibration suppression strategy [5–7].

The existing high-precision and high-dynamic response manipulators are mostly driven by the permanent magnet servo system. The translational flexible manipulator system (TFMS) driven by the permanent magnet motor is

a complex electromechanical system with a multimodule structure and multiphysical process [8–10]. On the SMT assembly line, owing to the fact that the size and quality of the electronic chips vary, the TFMS has variable load conditions during the operation process. Moreover, because of the structural characteristics of the flexible manipulator, the variable load conditions have significant influence on the dynamic characteristics of the TFMS and the performance of the corresponding vibration controller. The dynamic characteristic of a Cartesian manipulator with an end effector was studied in [11], and the results showed that the end effector placed at various locations may cause catastrophic failure. Similarly, under external and parametric excitations, Hamed et al. analyzed the nonlinear resonance and stability of the Cartesian manipulator with an intermediate end effector [12]. A mass ratio was defined in [13], and it was seen that the saddle-node bifurcation point of the frequency response curve for the subharmonic resonance of a visco-elastic Cartesian manipulator tended to decrease with the increase of the mass ratio. Because of the low stiffness and heavy deflection, the modal characteristics of the flexible manipulator are easily affected by load factors. Thus, when the elastic vibration controller of the TFMS is designed, the effect of terminal load should be considered comprehensively.

Fortunately, the full-state feedback controller can significantly improve the system dynamic characteristics by arbitrarily configuring the system closed-loop poles. On the basis of a zero set concept, a robust state feedback controller was presented for the STATCOM state feedback design [14]. The full-state feedback controller and output feedback controller were applied to a rehabilitation robot for the system uncertainties, and the results showed that the designed controller can effectively track the desired trajectory [15]. Aiming at the general linear heterodirectional hyperbolic systems, the state feedback regulator for the backstepping-based solution was designed [16]. When there are variable load conditions, the closed-loop poles of the TFMS can be configured by the state feedback controller to realize the effective control of the elastic vibration. However, the state feedback controller is essentially a closed-loop feedback controller, which inevitably suffers from the contradiction between the overshoot and the accuracy of the system response [17–19]. On the contrary, the state feedback controller has hysteresis in the vibration control of the TFMS, which means that the output signal of the drive end has already aroused the system mode vibration, and then the controller is used to adjust it. In order to solve the above problems, it is necessary to design the parameters of the closed-loop feedback controller to achieve the multiobjective optimization of the system response speed and overshoot, which increases the difficulty of the design of the state feedback controller itself.

The input shaping method is a typical feedforward control method. Through the convolution of the system input with a series of pulse signals, the new system input control signal, among which the frequency component that can arouse the system oscillation is filtered, can be generated to drive the original system. With the exact boundary conditions considered, the input shaping method was combined with the PD controller to suppress the residual vibration of a flexible-link parallel manipulator [20]. In [21], by using the S-type command, the modified input shaping was applied to realize the point-to-point motion of a modularized cable-suspended robot. A novel gripper was presented in [22], and the input shaping method was used to control the system residual vibration. Compared with the closed-loop control method, the input shaping method can adjust the system input in advance and has the ability of suppressing the system overshoot significantly. However, the input shaping method is essentially an open-loop control method which has poor adaptability under variable load conditions. Thus, it requires further research on how to combine the state feedback controller and the input shaper and apply it to the vibration control of the TFMS.

Above all, for the purpose of improving the robustness, rapidity, and accuracy of the vibration controller under variable load conditions, the combination mode of the state feedback controller and the input shaper is investigated to constitute the master-slave integrated controller for the elastic vibration of the TFMS. In the specific design process, with the inherent static difference considered, the state feedback controller is integrated with the integral controller to form the state feedback integral controller (SFIC). Moreover, based on the optimal algorithm and the cascade method, the two-mode vibration cascade shaper of the TFMS is designed, which can effectively relieve the time-delay effect of the conventional input shaper. The structure of this paper is organized as follows: Section 2 gives the dynamic modelling and decoupling analysis of the TFMS. The main contribution of this paper is presented in Section 3, which shows the design of the master-slave integrated controller for the elastic vibration of the TFMS. Simulation analysis is carried out in Section 4. The conclusions are summarized in Section 5.

2. Dynamic Modelling and Decoupling Analysis

The motion diagram of the TFMS is shown in Figure 1, where $\omega_y(x, t)$ is the transverse vibration of P point on the flexible manipulator, m_t indicates the quality of terminal load, and $Z(t)$ is the displacement of the base. The AC servomotor drives the base through the coupling and the ball screw pair, and then the flexible manipulator, which is rigidly connected with the base, can be driven to complete the specified operation. It is seen that the AC servomotor drives the flexible manipulator while exciting its elastic vibration. In the modelling process, the assumptions are made as follows: (i) the connection between the base and the flexible manipulator is purely rigid; (ii) the transmission gap of the transmission system is neglected; (iii) the flexible manipulator is equivalent to the Euler–Bernoulli beam and only the transverse vibration is considered; and (iv) the flexible manipulator moves on the horizontal plane and the influences of gravity and air damping force are ignored.

Taking the center of the base as the coordinate origin, the transverse absolute coordinates of the P point can be expressed as

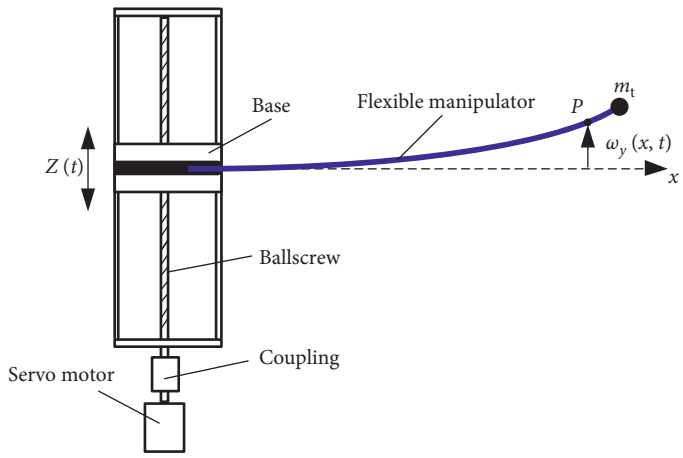

Figure 1: Motion diagram of the TFMS.

$$Y(x,t) = Z(t) + \omega_y(x,t). \tag{1}$$

The kinetic energy of the TFMS includes the kinetic energy of the base, the kinetic energy of the flexible manipulator, and the kinetic energy of the terminal load, which can be shown as

$$\begin{aligned} T_e &= \frac{1}{2}m_b\dot{Z}^2(t) + \frac{1}{2}\int_0^L \rho A\dot{Y}^2(x,t)dx + \frac{1}{2}m_t\dot{Y}^2(L,t) \\ &= \frac{1}{2}m_b\dot{Z}^2(t) + \frac{1}{2}\int_0^L \rho A\left[\dot{Z}(t) + \dot{\omega}_y(x,t)\right]^2 dx \\ &\quad + \frac{1}{2}m_t\left[\dot{Z}(t) + \dot{\omega}_y(L,t)\right]^2, \end{aligned} \tag{2}$$

where m_b is the mass of the base and ρ, A, and L are the density, the cross-sectional area, and the length of the flexible manipulator, respectively. The derivative notations are defined as $\dot{\Delta} = \partial(\Delta)/\partial t$.

The potential energy of the TFMS mainly considers the elastic potential energy generated by the deformation of the flexible manipulator, which can be represented as

$$U_e = \frac{1}{2}\int_0^L EI\left[\frac{\partial^2\omega_y(x,t)}{\partial x^2}\right]^2 dx, \tag{3}$$

where E and I are the modulus of elasticity and the moment of inertia of the flexible manipulator, respectively.

The external force of the TFMS mainly includes the driving force transmitted by the AC servomotor through the ball screw pair and the friction resistance between the base and the moving guide rail. In addition, the structural damping force of the flexible manipulator itself also needs to be considered. The direction of the driving force is along the motion direction of the base, while the directions of the friction and the structural damping force are opposite. Then, according to the virtual work principle [23, 24], the external virtual work of the TFMS can be shown as

$$\sigma W_e = F(t)\sigma Z(t) - R_f\dot{Z}(t)\sigma Z(t) - \mu_s\int_0^L \dot{\omega}_y(x,t)\sigma\omega_y(x,t)dx, \tag{4}$$

where $F(t)$ is the driving force of the base, R_f is the friction coefficient between the base and the moving guide rail, and μ_s indicates the structural damping of the flexible manipulator itself.

Based on Hamilton's principle [25, 26], the relationship among the kinetic energy, the potential energy, and the virtual work of the TFMS can be written as

$$\int(\delta T_e - \delta U_e + \delta W_e)dt = 0. \tag{5}$$

Substitution equations (1)–(4) into equation (5) yields

$$\begin{aligned} &(m_b + m_t + \rho AL)\ddot{Z}(t) + m_t\frac{\partial^2\omega_y(L,t)}{\partial t^2} + \int_0^L \rho A\frac{\partial^2\omega_y(x,t)}{\partial t^2}dx \\ &= F(t) - R_f\dot{Z}(t), \end{aligned} \tag{6}$$

$$\rho A\left[\ddot{Z}(t) + \frac{\partial^2\omega_y(x,t)}{\partial t^2}\right] + EI\frac{\partial^4\omega_y(x,t)}{\partial x^4} + \mu_s\dot{\omega}_y(x,t) = 0. \tag{7}$$

Equations (6) and (7) are a set of partial differential equations, which are difficult to be solved and are not convenient for the design of the vibration controller. Here, the assumed mode method is used to decouple the spatial and temporal scales of the elastic vibration of the flexible manipulator [27, 28]. Then, the transverse vibration of the flexible manipulator can be further expressed as

$$\omega_y(x,t) = \sum_{i=1}^{\infty}\phi_i(x)q_i(t), \tag{8}$$

where $\phi_i(x)$ is the i-th modal shape of the TFMS and $q_i(t)$ denotes the corresponding modal coordinates.

Because the root of the flexible manipulator is rigidly connected with the base, the boundary condition at the root is a fixed constraint: the deflection and the rotation angle are both 0. On the contrary, the end of the flexible manipulator is regarded as a free boundary condition: the bending moment and the shear force are both 0. Thus, the mode shape function of the flexible manipulator can be further shown as [29]

$$\phi_i(x) = \sin\beta_i x - \sinh\beta_i x - \frac{\sin\beta_i L + \sinh\beta_i L}{\cosh\beta_i L + \cos\beta_i L} \cdot (\cos\beta_i x - \cosh\beta_i x), \tag{9}$$

where β_i is a constant which is determined by the boundary conditions of the flexible manipulator and can be calculated by the equation $\cos\beta_i L \cosh\beta_i L = -1$.

With equation (8) combined, it is known from the relationship of structural mechanics that

$$EI\frac{\partial^4\phi_i(x)}{\partial x^4} = \rho A w_i^2, \tag{10}$$

where w_i is the i-th modal frequency of the flexible manipulator.

Substituting equations (8) and (10) into equations (6) and (7), one can obtain

$$(m_b + m_t + \rho AL)\ddot{Z}(t) + \sum_{i=1}^{\infty}\left[m_t\phi_i(L) + \rho A\int_0^L \phi_i(x)dx\right]\ddot{q}_i(t) = F(t) - R_f\dot{Z}(t), \tag{11}$$

$$\rho A\ddot{Z}(t) + \sum_{i=1}^{\infty}\left[\rho A\phi_i(x)\ddot{q}_i(t) + \rho A w_i^2 q_i(t) - \mu_{si}\phi_i(x)\dot{q}_i(t)\right] = 0, \tag{12}$$

where μ_{si} is the structural damping of the i-th mode for the flexible manipulator.

Through multiplying both sides of equation (12) by $\phi_j(x)$ and integrating along the length of the flexible manipulator, the dynamic model of the TFMS with spatial scale and time scale decoupled can be shown as

$$\begin{cases} (m_b + m_t + \rho AL)\ddot{Z}(t) + R_f\dot{Z}(t) \\ \quad + \sum_{i=1}^{\infty}\left[m_t\phi_i(L) + \rho A\int_0^L \phi_i(x)dx\right]\ddot{q}_i(t) = F(t), \\ \int_0^L \rho A\phi_1(x)dx\ddot{Z}(t) + \rho A\ddot{q}_1(t) + \rho A w_1^2 q_1(t) + \mu_{s1}\dot{q}_1(t) = 0, \\ \int_0^L \rho A\phi_2(x)dx\ddot{Z}(t) + \rho A\ddot{q}_2(t) + \rho A w_2^2 q_2(t) + \mu_{s2}\dot{q}_2(t) = 0, \\ \vdots \\ \int_0^L \rho A\phi_i(x)dx\ddot{Z}(t) + \rho A\ddot{q}_i(t) + \rho A w_i^2 q_i(t) + \mu_{si}\dot{q}_i(t) = 0. \end{cases} \tag{13}$$

3. Control Design

3.1. Design of the SFIC. According to the existing research, on the flexible manipulator, whose length is much larger than its cross-sectional area, the first several low-order modes play a leading role in the system vibration responses. And taking the first two order modes can completely meet the control requirements for the TFMS [30, 31]. In order to facilitate the design and analysis of the SFIC, the state variables are taken as $\mathbf{x}_t = \begin{bmatrix} Z & q_1 & q_2 & \dot{Z} & \dot{q}_1 & \dot{q}_2 \end{bmatrix}^T$. Then, equation (13) can be represented as a state-space model, which is shown as

$$\begin{cases} \dot{x}_t = \mathbf{A}\mathbf{x}_t + \mathbf{B}u_t, \\ y_t = \mathbf{C}\mathbf{x}_t + \mathbf{D}u_t, \end{cases} \tag{14}$$

where

$$\begin{aligned} \mathbf{A} &= \begin{bmatrix} \mathbf{0} & \mathbf{I} \\ \mathbf{M}^{-1}\mathbf{K} & \mathbf{M}^{-1}\mathbf{H} \end{bmatrix}, \\ \mathbf{B} &= \begin{bmatrix} \mathbf{0} \\ \mathbf{M}^{-1}\mathbf{\Lambda} \end{bmatrix}, \\ \mathbf{C} &= \begin{bmatrix} 1 & 0 & \cdots & 0 \\ 0 & 1 & \ddots & \vdots \\ \vdots & \ddots & \ddots & 0 \\ 0 & \cdots & 0 & 1 \end{bmatrix}_{6*6}, \\ \mathbf{D} &= \begin{bmatrix} 0 \\ \vdots \\ 0 \end{bmatrix}_{6*1}, \\ u_t &= F(t), \\ \mathbf{M} &= \begin{bmatrix} m_b + \rho AL & m_1 & m_2 \\ m_1 & \rho A & 0 \\ m_2 & 0 & \rho A \end{bmatrix}, \\ \mathbf{K} &= \begin{bmatrix} 0 & 0 & 0 \\ 0 & -\rho A w_1^2 & 0 \\ 0 & 0 & -\rho A w_2^2 \end{bmatrix}, \\ \mathbf{\Lambda} &= \begin{bmatrix} 1 \\ 0 \\ 0 \end{bmatrix}, \\ \mathbf{H} &= \begin{bmatrix} -R_f & 0 & 0 \\ 0 & -\mu_{s1} & 0 \\ 0 & 0 & -\mu_{s2} \end{bmatrix}, \\ m_1 &= \int_0^L \rho A\phi_1(x)dx, \\ m_2 &= \int_0^L \rho A\phi_2(x)dx. \end{aligned} \tag{15}$$

Based on the system controllability and observability theory, one can obtain that the state variables of the TFMS are completely controllable and observable [32, 33]. Then, with our previous work on the design of the two-time-scale observer for the flexible manipulator combined [31], the SFIC of the TFMS is constructed and shown in Figure 2, where $Y_r(L, t)$ is the expected displacement of the end of the TFMS, $\mathbf{K}_z$ is the gain matrix of the state feedback controller, K_i is the coefficient of the integral controller, and $\widehat{\Delta}$ represents the observation value of the corresponding quantity. The SFIC of the TFMS mainly includes three parts: the two-time-scale observer, the state feedback controller, and the integral controller. The two-time-scale observer, including the speed observer and the vibration observer, is designed to achieve the estimation

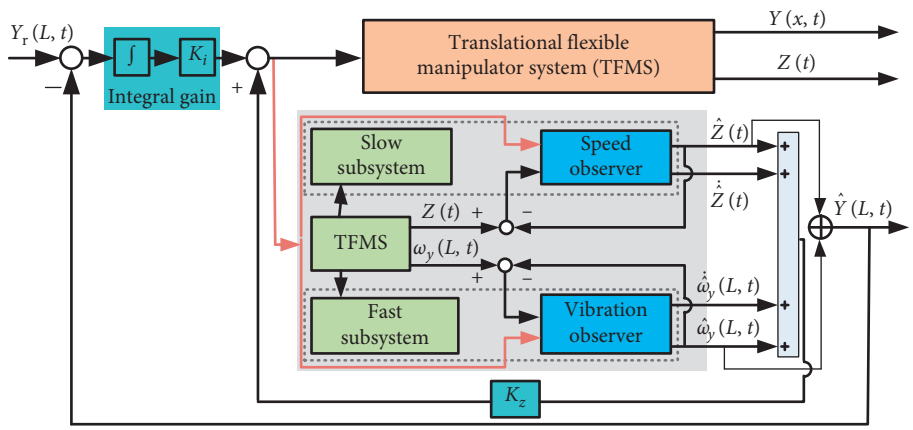

Figure 2: State feedback integral controller of the TFMS.

for the vibration signals, and their time derivative of the TFMS as well as the speed observer and the vibration observer is separately designed for the slow and fast subsystems which are decomposed from the dynamic model of the TFMS by the singular perturbation. The two-time-scale observer provides necessary status information for the state feedback controller to realize the state regulation for the TFMS. Moreover, the state feedback controller is combined with the integral controller for solving the inherent static difference.

The error vector of the desired displacement at the end of the TFMS is defined as

$$\dot{p}(t) = e(t) = Y_r(L,t) - \hat{Y}(L,t). \tag{16}$$

Then, the output control quantity of the SFIC can be expressed as

$$u_t(t) = \mathbf{K}_z \hat{\mathbf{x}}_t(t) + K_i \int e(t)dt = \begin{bmatrix} \mathbf{K}_z & K_i \end{bmatrix} \begin{bmatrix} \hat{\mathbf{x}}_t(t) \\ p(t) \end{bmatrix}. \tag{17}$$

In order to prove that the designed SFIC can drive the TFMS to a specified position without static error, the end positioning error of the flexible manipulator is added as a new state variable. And the augmented system can be shown as

$$\begin{cases} \begin{bmatrix} \dot{\hat{\mathbf{x}}}_t(t) \\ \dot{p}(t) \end{bmatrix} = \begin{bmatrix} \mathbf{A} & 0 \\ -\mathbf{C}_4\mathbf{C} & 0 \end{bmatrix} \begin{bmatrix} \hat{\mathbf{x}}_t(t) \\ p(t) \end{bmatrix} + \begin{bmatrix} \mathbf{B} \\ 0 \end{bmatrix} u_t \\ \quad + \begin{bmatrix} \mathbf{K}_e \\ 0 \end{bmatrix} \mathbf{C}_1 \hat{\mathbf{x}}_t(t) + \begin{bmatrix} d(t) \\ Y_r(L,t) \end{bmatrix}, \\ Y(L,t) = \hat{Y}(L,t) = \begin{bmatrix} \mathbf{C}_4\mathbf{C} & 0 \end{bmatrix} \begin{bmatrix} \hat{\mathbf{x}}_t(t) \\ p(t) \end{bmatrix}, \end{cases} \tag{18}$$

where $\mathbf{C}_1 = [1\ 0\ 0\ 0\ 0\ 0]$, $\mathbf{C}_4 = [1\ \phi_1(L)\ \phi_2(L)\,0\,0\,0]$, $\mathbf{K}_e = [\mathbf{K}_s\ \ \mathbf{K}_f]^T$, and $d(t)$ is the external interference of the TFMS.

Equation (17) is substituted into equation (18), and the Laplace transform is carried out for the result. Then, according to the terminal value theorem, the steady-state value for the augmented TFMS can be obtained as

$$\begin{aligned} \lim_{t\to 0} \begin{bmatrix} \mathbf{x}_t(t) \\ p(t) \end{bmatrix} &= \lim_{S\to 0} S \left(S\mathbf{I} - \begin{bmatrix} \mathbf{A} - \mathbf{K}_e\mathbf{C} + \mathbf{B}\mathbf{K}_z + \mathbf{K}_e\mathbf{C}_1 & \mathbf{B}K_i \\ -\mathbf{C}_4\mathbf{C} & 0 \end{bmatrix} \right)^{-1} \\ &\quad \cdot \begin{bmatrix} \dfrac{d(S)}{S} \\ \dfrac{-Y_r(L,S)}{S} \end{bmatrix} \\ &= \begin{bmatrix} \mathbf{A} - \mathbf{K}_e\mathbf{C} + \mathbf{B}\mathbf{K}_z + \mathbf{K}_e\mathbf{C}_1 & \mathbf{B}K_i \\ -\mathbf{C}_4\mathbf{C} & 0 \end{bmatrix}^{-1} \begin{bmatrix} d_0 \\ -Y_{r0} \end{bmatrix}, \end{aligned} \tag{19}$$

where S is the symbol of the Laplace transform.

According to equation (19), $p(t)$ tends to be constant, which means that the system error vector tends to 0. Then, the static error of the desired displacement at the end of the TFMS can be shown as

$$\lim_{t\to\infty} \left(Y_r(L,t) - \hat{Y}(L,t) \right) = \lim_{t\to\infty} \dot{p}(t) = 0. \tag{20}$$

Through the above analysis, by designing a suitable state feedback control law for the augmented TFMS, the purpose of positioning the flexible manipulator to a specified position without deviation is achieved.

Based on the pole assignment method, the control parameters of the SFIC are designed. Because the first two modes of the transverse vibration of the flexible manipulator are considered, there are 7 poles in the augmented TFMS. Moreover, owing to the fact that the vibration frequency and damping of the transverse vibration mode coordinates are much smaller than the vibration frequency and damping of the base, the response of the augmented TFMS is mainly determined by the two pairs of poles corresponding to the vibration mode coordinates, and the other three poles are fast poles. According to equation (18), the system matrix and input matrix for the augmented TFMS can be expressed as

$$\mathbf{A}_g = \begin{bmatrix} \mathbf{A} & 0 \\ -\mathbf{C}_4\mathbf{C} & 0 \end{bmatrix}, \quad \mathbf{B}_g = \begin{bmatrix} \mathbf{B} \\ 0 \end{bmatrix}. \tag{21}$$

The expected poles for the augmented TFMS are assumed as $[\lambda_1\ \lambda_2\ \lambda_3\ \lambda_4\ \lambda_5\ \lambda_6\ \lambda_7]$. The first four are the two pairs of poles that play a leading role in the transverse vibration of the flexible manipulator, and the other three are fast poles. Then, the characteristic polynomial for the augmented TFMS can be deduced as

$$\begin{aligned} f_1(\lambda) &= (\lambda-\lambda_1)(\lambda-\lambda_2)(\lambda-\lambda_3)(\lambda-\lambda_4)(\lambda-\lambda_5)(\lambda-\lambda_6)(\lambda-\lambda_7) \\ &= \ell_0\lambda^7 + \ell_1\lambda^6 + \ell_2\lambda^5 + \ell_3\lambda^4 + \ell_4\lambda^3 + \ell_5\lambda^2 + \ell_6\lambda + \ell_7, \end{aligned} \tag{22}$$

where ℓ_0, ℓ_1, ℓ_2, ℓ_3, ℓ_4, ℓ_5, ℓ_6, and ℓ_7 are the constant coefficients related to the expected poles.

In the augmented TFMS, the feedback gain matrix can be expressed as $\mathbf{K}_g = [\mathbf{K}_z\ \ K_i]^T$. Then, after introducing the SFIC, the system matrix for the augmented TFMS can be shown as $\mathbf{A}_{gc} = \mathbf{A}_g - \mathbf{B}_g\mathbf{K}_g$. With equation (22) combined, it is known that the system matrix for the augmented TFMS should satisfy

$$\begin{aligned} \varphi(\mathbf{A}_{gc}) = {} & \ell_0(\mathbf{A}_g - \mathbf{B}_g\mathbf{K}_g)^7 + \ell_1(\mathbf{A}_g - \mathbf{B}_g\mathbf{K}_g)^6 + \ell_2(\mathbf{A}_g - \mathbf{B}_g\mathbf{K}_g)^5 \\ & + \ell_3(\mathbf{A}_g - \mathbf{B}_g\mathbf{K}_g)^4 + \ell_4(\mathbf{A}_g - \mathbf{B}_g\mathbf{K}_g)^3 \\ & + \ell_5(\mathbf{A}_g - \mathbf{B}_g\mathbf{K}_g)^2 + \ell_6(\mathbf{A}_g - \mathbf{B}_g\mathbf{K}_g) + \ell_7. \end{aligned} \tag{23}$$

Finally, according to Ackermann's formula, the gains of the SFIC can be expressed as

$$\mathbf{K}_g = \mathbf{C}_2[\mathbf{B}_g\ \ \mathbf{A}_g\mathbf{B}_g\ \ \mathbf{A}_g^2\mathbf{B}_g\ \ \mathbf{A}_g^3\mathbf{B}_g\ \ \mathbf{A}_g^4\mathbf{B}_g\ \ \mathbf{A}_g^5\mathbf{B}_g\ \ \mathbf{A}_g^6\mathbf{B}_g]\varphi(\mathbf{A}_g), \tag{24}$$

where $\mathbf{C}_2 = [0\ 0\ 0\ 0\ 0\ 0\ 1]$.

3.2. Design of the Two-Mode Vibration Cascade Shaper. Because of the time-delay link, the conventional input shaper will significantly affect the response speed of the TFMS. Thus, based on the input shaping method and the optimal theory, the two-mode vibration cascade shaper of the TFMS is designed for reducing the time-lag effect introduced by the input shaper [34].

The two-mode vibration cascade shaper is cascaded by the first-mode vibration shaper and the second-mode vibration shaper of the TFMS. Moreover, the first two modes of vibration shapers for the TFMS are designed separately, and the first mode is illustrated as an example. The system state variables in equation (14) are reselected as $\mathbf{x}_m = [q_1\ \ \dot{q}_1]^T$, and the new state-space model can be obtained as

$$\begin{cases} \dot{x}_m = \mathbf{A}_m\mathbf{x}_m + \mathbf{B}_m u_m, \\ y_m = \mathbf{C}_m\mathbf{x}_m, \end{cases} \tag{25}$$

where

$$\begin{aligned} \mathbf{A}_m &= \begin{bmatrix} 0 & 1 \\ -w_1^2 & -2\xi_{m1}w_1 \end{bmatrix}, \\ \mathbf{B}_m &= \begin{bmatrix} 0 \\ -m_1 \end{bmatrix}, \\ \mathbf{C}_m &= [1\ \ 0], \\ u_m &= \ddot{Z}(t), \\ \xi_{m1} &= \frac{\mu_{s1}}{2\rho A w_1}. \end{aligned} \tag{26}$$

According to Duhamel's integral, the time-domain expression of equation (25) can be solved as

$$\mathbf{X}_m(t) = \mathbf{\Gamma}(t,t_0)\mathbf{X}_m(t_0) + \int_0^t \mathbf{\Gamma}(t,\hat{t})\mathbf{B}_m u_m(\hat{t})d\hat{t}, \tag{27}$$

where

$$\begin{aligned} \mathbf{\Gamma}(t,\hat{t}) &= \begin{bmatrix} \Gamma(1,1) & \Gamma(1,2) \\ \Gamma(2,1) & \Gamma(1,2) \end{bmatrix}, \\ \Gamma(1,1) &= \exp(-\xi_{m1}w_1(t-\hat{t}))\left\{\cos\left[w_1\sqrt{1-\xi_{m1}^2}\,(t-\hat{t})\right]\right. \\ &\quad \left. + \frac{\xi_{m1}}{\sqrt{1-\xi_{m1}^2}}\sin\left[w_1\sqrt{1-\xi_{m1}^2}\,(t-\hat{t})\right]\right\}, \\ \Gamma(1,2) &= \frac{1}{w_1\sqrt{1-\xi_{m1}^2}}\exp(-\xi_{m1}w_1(t-\hat{t})) \\ &\quad \cdot \sin\left[w_1\sqrt{1-\xi_{m1}^2}\,(t-\hat{t})\right], \\ \Gamma(1,2) &= -\frac{w_1}{\sqrt{1-\xi_{m1}^2}}\exp(-\xi_{m1}w_1(t-\hat{t})) \\ &\quad \cdot \sin\left[w_1\sqrt{1-\xi_{m1}^2}\,(t-\hat{t})\right], \\ \Gamma(2,2) &= \exp(-\xi_{m1}w_1(t-\hat{t}))\left\{\cos\left[w_1\sqrt{1-\xi_{m1}^2}\,(t-\hat{t})\right]\right. \\ &\quad \left. - \frac{\xi_{m1}}{\sqrt{1-\xi_{m1}^2}}\sin\left[w_1\sqrt{1-\xi_{m1}^2}\,(t-\hat{t})\right]\right\}. \end{aligned} \tag{28}$$

Combined with the requirement of the terminal positioning error, the quadratic objective function of the TFMS is set as

$$J_m(t) = \frac{1}{2}\mathbf{X}_m^T(t)\mathbf{W}_m\mathbf{X}_m(t), \tag{29}$$

where $\mathbf{W}_{\mathrm{m}}$ is the weighted matrix.

To the first-mode vibration of the flexible manipulator, the number of pulses of the first-mode vibration shaper is set as 2 and the amplitude and the time lag of the first pulse are set as $A_1^{\mathrm{s}} = 1$ and $t_1^{\mathrm{s}} = 0$. Then, equation (29) can be further expressed as

$$J_{\mathrm{m}}(t) = \frac{1}{2}\left[\mathbf{\Gamma}(t,0)\mathbf{B}_{\mathrm{m}} + \mathbf{\Gamma}\left(t,t_2^{s}\right)\mathbf{B}_{\mathrm{m}}A_2^{\mathrm{s}}\right]^{\mathrm{T}}\mathbf{W}_{\mathrm{m}}\left[\mathbf{\Gamma}(t,0)\mathbf{B}_{\mathrm{m}} + \mathbf{\Gamma}\left(t,t_2^{\mathrm{s}}\right)\mathbf{B}_{\mathrm{m}}A_2^{\mathrm{s}}\right]. \tag{30}$$

Based on the optimal theory, in order to minimize the objective function, two conditions, $\partial J_{\mathrm{m}}(t)/\partial A_2^{\mathrm{s}} = 0$ and $\partial J_{\mathrm{m}}(t)/\partial (A_2^{\mathrm{s}})^2 = 0$, need to be met at the same time. Then, one can obtain

$$A_2^{\mathrm{s}} = -2\exp\left(-\xi_{\mathrm{m}}w_1t_2^{\mathrm{s}}\right)\cos\left(2w_1\sqrt{1-\xi_{\mathrm{m}}^2}\right)t_2^{\mathrm{s}}. \tag{31}$$

According to the amplitude and time lag of the first pulse in the first-mode vibration shaper, by combining with equation (31) and normalization processing, one can obtain

$$G_{\mathrm{shape}}(S) = A_1^{\mathrm{s}} + A_2^{\mathrm{s}}\exp\left(-t_2^{\mathrm{s}}S\right). \tag{32}$$

The amplitude of the corresponding pulse in equation (31) can be expressed as

$$\begin{cases} A_1^{\mathrm{s}} = \dfrac{1}{1-2\cos\left(w_1\sqrt{1-\xi_{\mathrm{m}}^2}\,t_2^{\mathrm{s}}\right)\exp\left(-\xi_{\mathrm{m}}w_1t_2^{\mathrm{s}}\right)}, \\ A_2^{\mathrm{s}} = -\dfrac{2\cos\left(w_1\sqrt{1-\xi_{\mathrm{m}}^2}\,t_2^{\mathrm{s}}\right)\exp\left(-\xi_{\mathrm{m}}w_1t_2^{\mathrm{s}}\right)}{1-2\cos\left(w_1\sqrt{1-\xi_{\mathrm{m}}^2}\,t_2^{\mathrm{s}}\right)\exp\left(-\xi_{\mathrm{m}}w_1t_2^{\mathrm{s}}\right)}. \end{cases} \tag{33}$$

On the contrary, it is obvious that the zero points of equation (32) cover the poles of the original system, which is also the reason why the designed mode vibration shaper can effectively alleviate the time-lag effect of the conventional input shaper. Thus, the time lag (t_2^{s}) in equation (32) can be selected arbitrarily.

Similarly, the control parameters of the second-mode vibration shaper for the flexible manipulator can be determined. According to equation (33), the first-mode vibration shaper and the second-mode vibration shaper are designed as

$$G_{\mathrm{OP\_shape1}} = \begin{bmatrix} A_{11}^{\mathrm{s}} & A_{12}^{\mathrm{s}} \\ 0 & t_{12}^{\mathrm{s}} \end{bmatrix}, \tag{34}$$

$$G_{\mathrm{OP\_shape2}} = \begin{bmatrix} A_{21}^{\mathrm{s}} & A_{22}^{\mathrm{s}} \\ 0 & t_{22}^{\mathrm{s}} \end{bmatrix}, \tag{35}$$

where A_{11}^{s} and A_{12}^{s} are the amplitudes of the corresponding pulses for the first-mode vibration shaper, t_{12}^{s} is the time lag of the second pulse for the first-mode vibration shaper, A_{21}^{s} and A_{22}^{s} are the amplitudes of the corresponding pulses for the second-mode vibration shaper, and t_{22}^{s} is the time lag of the second pulse for the second-mode vibration shaper.

Based on the cascade method, the two-mode vibration cascade shaper of the TFMS can be deduced as

$$G_{\mathrm{TOP\_shape}} = \begin{bmatrix} A_{11}^{\mathrm{s}}A_{21}^{\mathrm{s}} & A_{11}^{\mathrm{s}}A_{22}^{\mathrm{s}} & A_{12}^{\mathrm{s}}A_{21}^{\mathrm{s}} & A_{12}^{\mathrm{s}}A_{22}^{\mathrm{s}} \\ 0 & t_{22}^{\mathrm{s}} & t_{12}^{\mathrm{s}} & t_{12}^{\mathrm{s}} + t_{22}^{\mathrm{s}} \end{bmatrix}, \tag{36}$$

where TOP means the two-mode vibration cascade shaper.

3.3. Design of the Master-Slave Integrated Controller. If the two-mode vibration cascade shaper is set in the closed loop of the SFIC, the time-lag link will affect the stability of the closed-loop system. Thus, in the designed master-slave integrated controller, the two-mode vibration cascade shaper is placed outside the closed loop of the SFIC, which is illustrated in Figure 3.

The design process of the master-slave integrated controller for the TFMS is as follows:

Step 1: with the angular frequencies and damping ratios of the first two modes of the flexible manipulator combined, the system expected poles are set up. And according to equation (24), the control gains of the SFIC are obtained.

Step 2: among the configured system poles, two pairs of poles that play a leading role in the transverse vibration of the flexible manipulator are extracted.

Step 3: the angular frequencies and damping ratios of the closed-loop system are calculated.

Step 4: the first-mode vibration shaper and the second-mode vibration shaper of the TFMS are designed by equation (33).

Step 5: the two-mode vibration cascade shaper of the TFMS is determined by equation (36).

Step 6: the master-slave integrated controller of the TFMS is constructed by the combination mode which is shown in Figure 3.

4. Simulation Verification

In this section, the master-slave integrated controller is verified by simulation experiment analysis. The physical parameters of the flexible manipulator are set as $L = 400$ mm, $\rho = 2030\,\mathrm{kg{\cdot}m^3}$, $E = 25.24$ GPa, and $A = 135\,\mathrm{mm^2}$. The simulation platform is constructed by MATLAB 2015b/Simulink.

4.1. Control Effect Analysis of the Two-Mode Vibration Cascade Shaper. Firstly, the movement for the base of the TFMS is set as trapezoidal velocity movement and the specific motion parameters are set as follows: a constant acceleration motion of $1250\,\mathrm{mm/s^2}$ during $t = 0$–0.2 s, a constant speed motion of 250 mm/s during $t = 0.2$–0.8 s, and a constant deceleration motion of $-1250\,\mathrm{mm/s^2}$ during $t = 0.8$–1.0 s. When the two-mode vibration cascade shaper is used alone, the velocity curves, before and after shaping, of the base are shown in Figure 4(a) and the displacement curves, before and after shaping, of the base are shown in Figure 4(b).

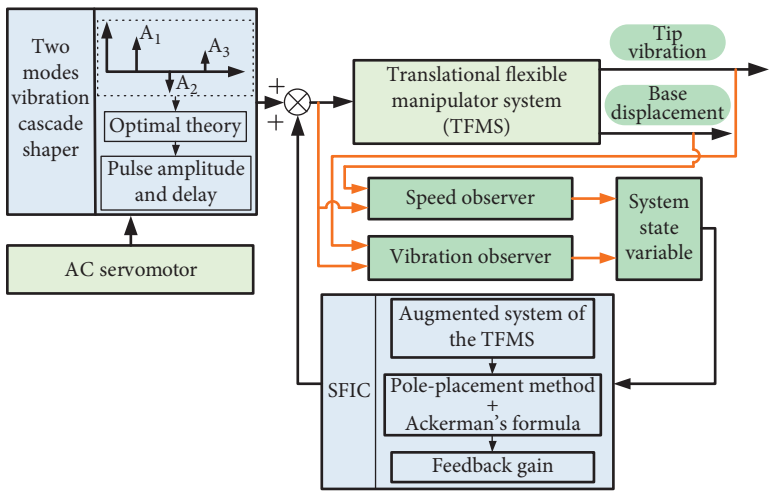

Figure 3: Elastic vibration integrated controller of the TFMS.

It is seen from Figure 4(b) that the output displacements, before and after using the two-mode vibration cascade shaper, of the base are consistent, which remain 200 mm. Then, the validity of the two-mode vibration cascade shaper is verified. It is known from Figure 4(a) that the speed curve of the base is transformed from a trapezoid curve to a ladder trapezoid curve after the time-lag filtering of the two-mode vibration cascade shaper.

Figure 5 shows the control effect of the two-mode vibration cascade shaper on the first-order mode coordinate of the flexible manipulator. From Figure 5(a), it is seen that the first-order mode coordinate of the flexible manipulator is suppressed effectively, which means that the two-mode vibration cascade shaper can remarkably filter out the frequency components, exciting the system vibration, in the input signal. On the contrary, under different terminal loads, the control results of the two-mode vibration cascade shaper are shown in Figure 5(b). It is known that the robustness of the two-mode vibration cascade shaper is poor and it cannot adapt to the variable load conditions of the TFMS. Thus, the SFIC should be added to construct the master-slave integrated controller for the TFMS.

4.2. Control Effect Analysis of the SFIC with Different Input Shapers Combined. According to the natural frequencies and damping ratios for the first two modes of the TFMS, the closed-loop poles of the augmented TFMS are configured. With the system response speed considered, the natural frequencies and damping ratios, which correspond to the two pairs of the system dominant poles, are set as 10.00 rad/s, 0.30 and 25.00 rad/s, 0.20. Then, the closed-loop poles of the augmented TFMS can be calculated as $[-3.00+9.54\mathbf{i}\ \ -3.00-9.54\mathbf{i}\ \ -5.0+24.49\mathbf{i}\ \ -5.0-24.49\mathbf{i}\ -50{-}51{-}52]$. On the basis of equation (24), the gains of the SFIC for the augmented TFMS are calculated as $[2.34\ \ 1.01\text{E}3\ \ 1.60\text{E}6\ \ 0.31\ \ 13.38\ \ -1.61\text{E}3\ \ 17.34]$. Then, according to equation (33), the control parameters of the first two modes of vibration shapers for the TFMS can be designed as

$$G_{\text{OP\_shape1}} = \begin{bmatrix} 1.2529 & -0.9014 \\ 0 & 0.1098 \end{bmatrix}, \quad G_{\text{OP\_shape2}} = \begin{bmatrix} 1.1840 & -0.9561 \\ 0 & 0.0428 \end{bmatrix}. \tag{37}$$

Furthermore, the parameters of the two-mode vibration cascade shaper of the TFMS can be calculated as

$$G_{\text{TOP\_shape}} = \begin{bmatrix} 1.4835 & -1.1980 & -1.0672 & 0.8618 \\ 0 & 0.0428 & 0.1098 & 0.1526 \end{bmatrix}. \tag{38}$$

Similarly, for the TFMS, in accordance with [35, 36], the two-mode ZV (TZV) shaper, two-mode ZVD (TZVD) shaper, and two-mode EI (TEI) shaper, for which the allowable residual oscillation amplitude is set at 3%, are calculated as

$$\begin{aligned} G_{\text{TZV\_shape}} &= \begin{bmatrix} 0.4773 & 0.2514 & 0.1777 & 0.0936 \\ 0 & 0.1283 & 0.3293 & 0.4576 \end{bmatrix}, \\ G_{\text{TZVD\_shape}} &= \begin{bmatrix} 0.23 & 0.24 & 0.06 & 0.17 & 0.18 & 0.05 & 0.03 & 0.03 & 0.009 \\ 0 & 0.13 & 0.26 & 0.33 & 0.46 & 0.59 & 0.66 & 0.79 & 0.92 \end{bmatrix}, \\ G_{\text{TEI\_shape}} &= \begin{bmatrix} 0.07 & 0.15 & 0.07 & 0.12 & 0.24 & 0.12 & 0.07 & 0.12 & 0.07 \\ 0 & 0.13 & 0.26 & 0.33 & 0.46 & 0.59 & 0.66 & 0.79 & 0.92 \end{bmatrix}. \end{aligned} \tag{39}$$

The target displacement of the base for the TFMS is set as 200 mm, and the control target is to locate the base to the designated position by suppressing the elastic vibration of the flexible manipulator quickly. The control effects of the above shapers are shown in Figure 6. As is shown in Figure 6(a), although the SFIC can control the base moving to the specified position, the overshoot of the base displacement can reach 40% when the requirement of fast positioning is satisfied, which is not allowed in the actual system. The actual reason is that the requirements of system rapidity and system overshoot are a pair of contradictory quantities, and the rapid response of the system will inevitably lead to the increase of system overshoot. On the contrary, when the SFIC is combined with the conventional

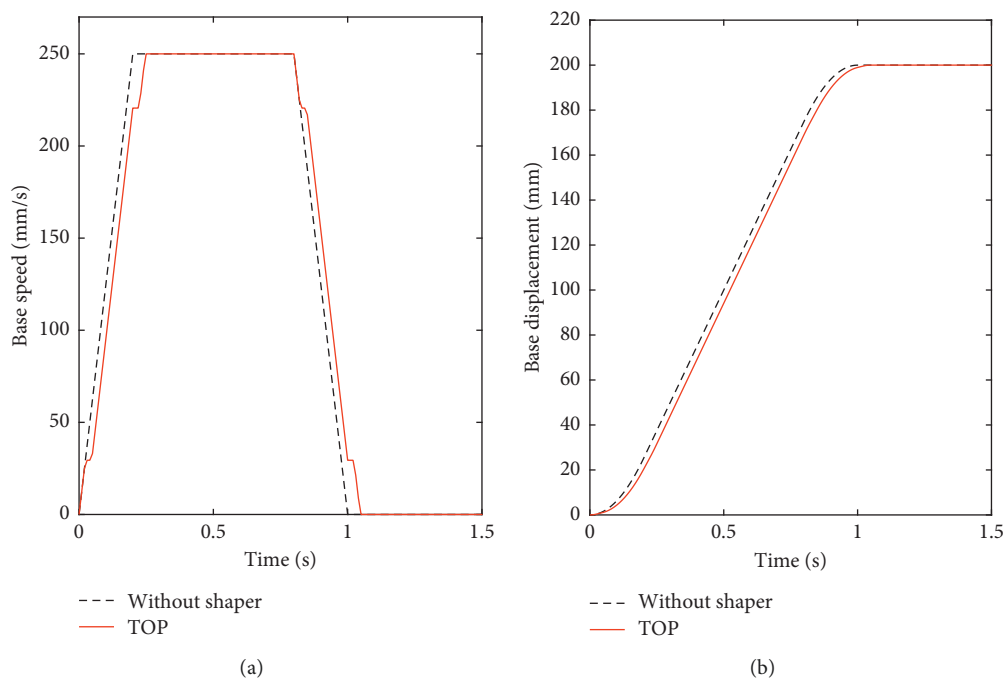

FIGURE 4: Positioning base velocity and displacement curves before and after the effect of the two-mode vibration cascade shaper: (a) velocity curve; (b) displacement curve.

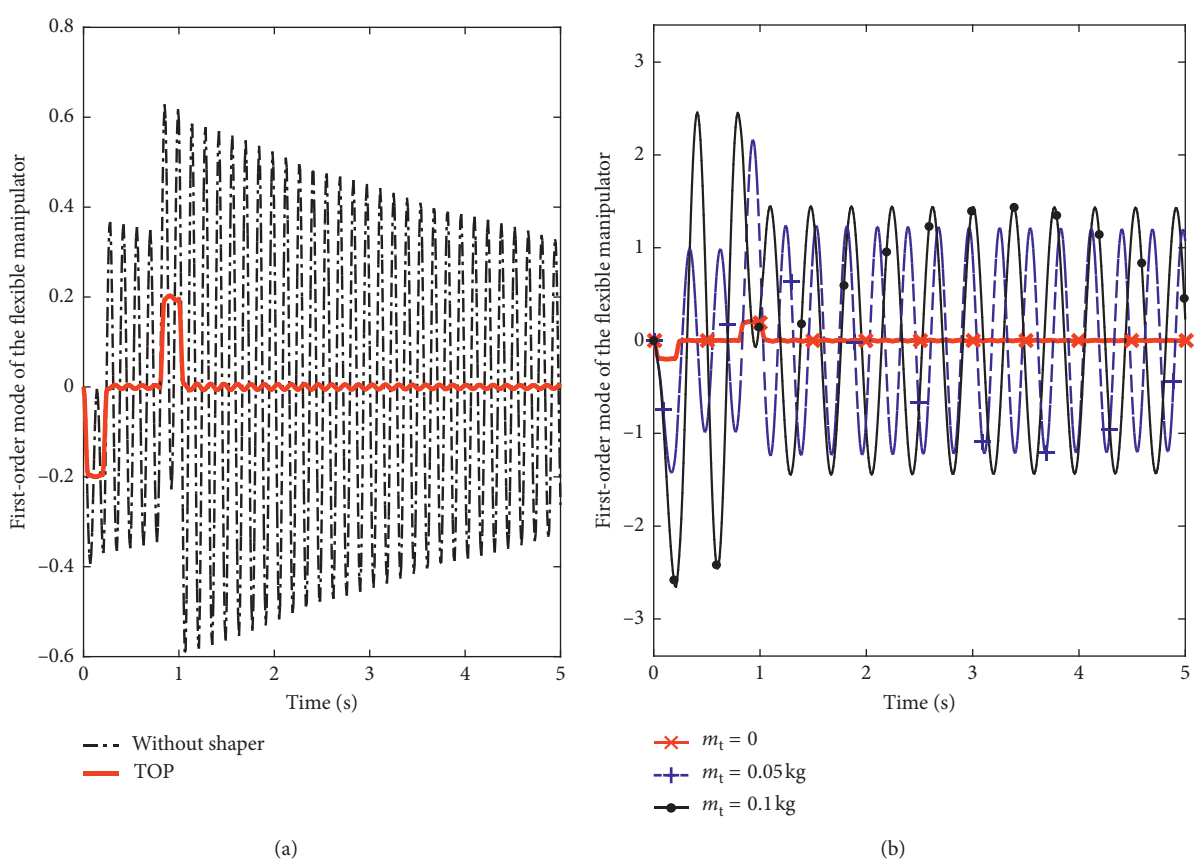

FIGURE 5: Control effect of the two-mode vibration cascade shaper on the elastic vibration of the flexible manipulator: (a) comparison of control effect before and after shaping; (b) control effect under different terminal loads.

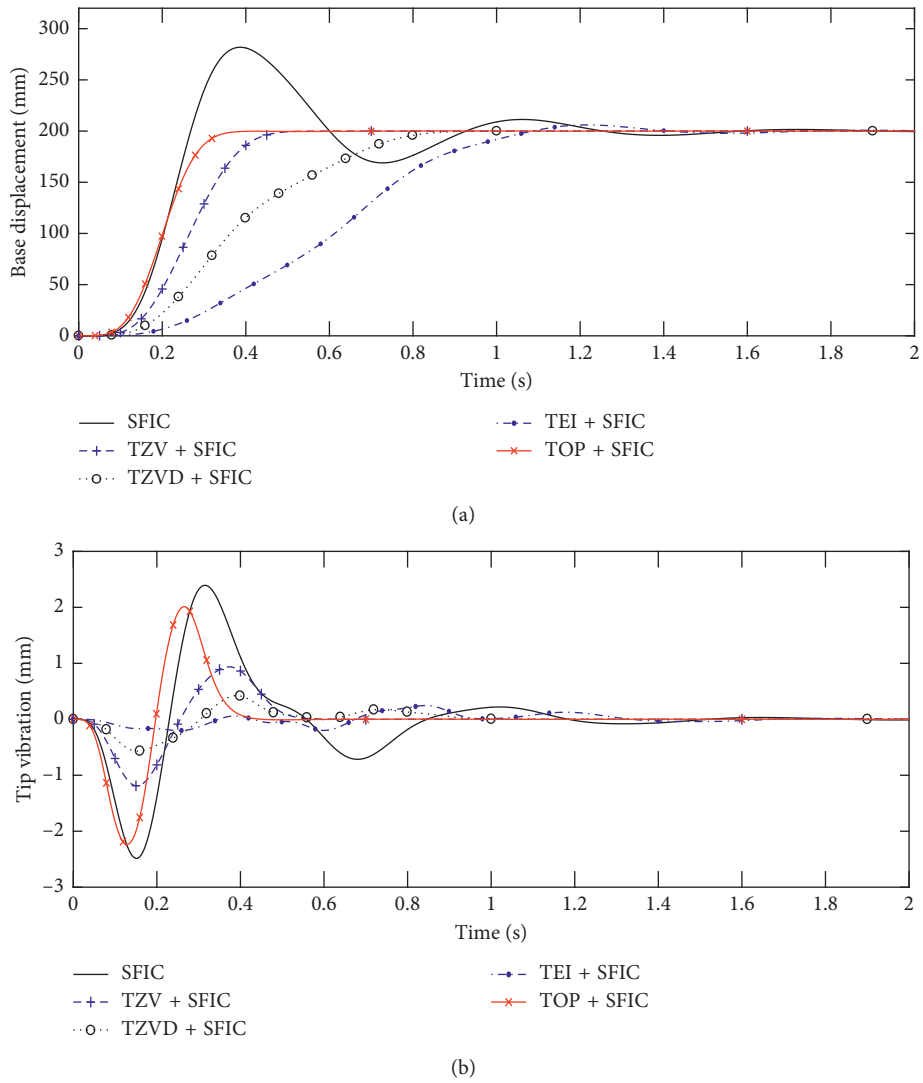

Figure 6: Control effect of the SFIC with different input shapers combined on the TFMS: (a) control effect of the base displacement; (b) control effect of the elastic vibration.

input shaper such as the TZV shaper, the system overshoot is effectively reduced, but the system response speed is reduced, which is caused by the time-lag effect of the conventional input shaper. Fortunately, the respond speed of the designed master-slave integrated controller is basically the same as that of the SFIC, while the system overshoot performance has been greatly improved. That being said, the system response speed and system rapidity can achieve synchronous optimization by combining the SFIC with the two-mode vibration cascade shaper.

Similarly, as is shown in Figure 6(b), compared with the conventional input shapers, the vibration suppression effect of the designed master-slave integrated controller is optimal. Moreover, through combining the SFIC with the TZV shaper, the TZVD shaper, the TEI shaper, and the designed two-mode vibration cascade shaper, it is seen from Figure 6 that the respond speed and vibration suppression speed of the designed master-slave integrated controller are the best, which also proves that the two-mode vibration cascade shaper can effectively improve the time-lag effect of the conventional input shapers.

4.3. Control Effect of the Master-Slave Integrated Controller under Variable Load Conditions. Figure 7 shows the control effect of the master-slave integrated controller under different terminal loads. It is seen from Figure 7(a) that the terminal load has no impact on the control effect of the master-slave integrated controller on the base displacement. Furthermore, as shown in Figure 7(b), under the action of the same control parameters, the master-slave integrated controller can effectively suppress the elastic vibration of the TFMS with different terminal loads. With Figures 5(b) and 7(b) compared, it is obvious that the designed master-slave integrated controller can efficaciously improve the robustness of the two-mode vibration cascade shaper.

Above all, through combining the two-mode vibration cascade shaper and the SFIC of the TFMS, the robustness of

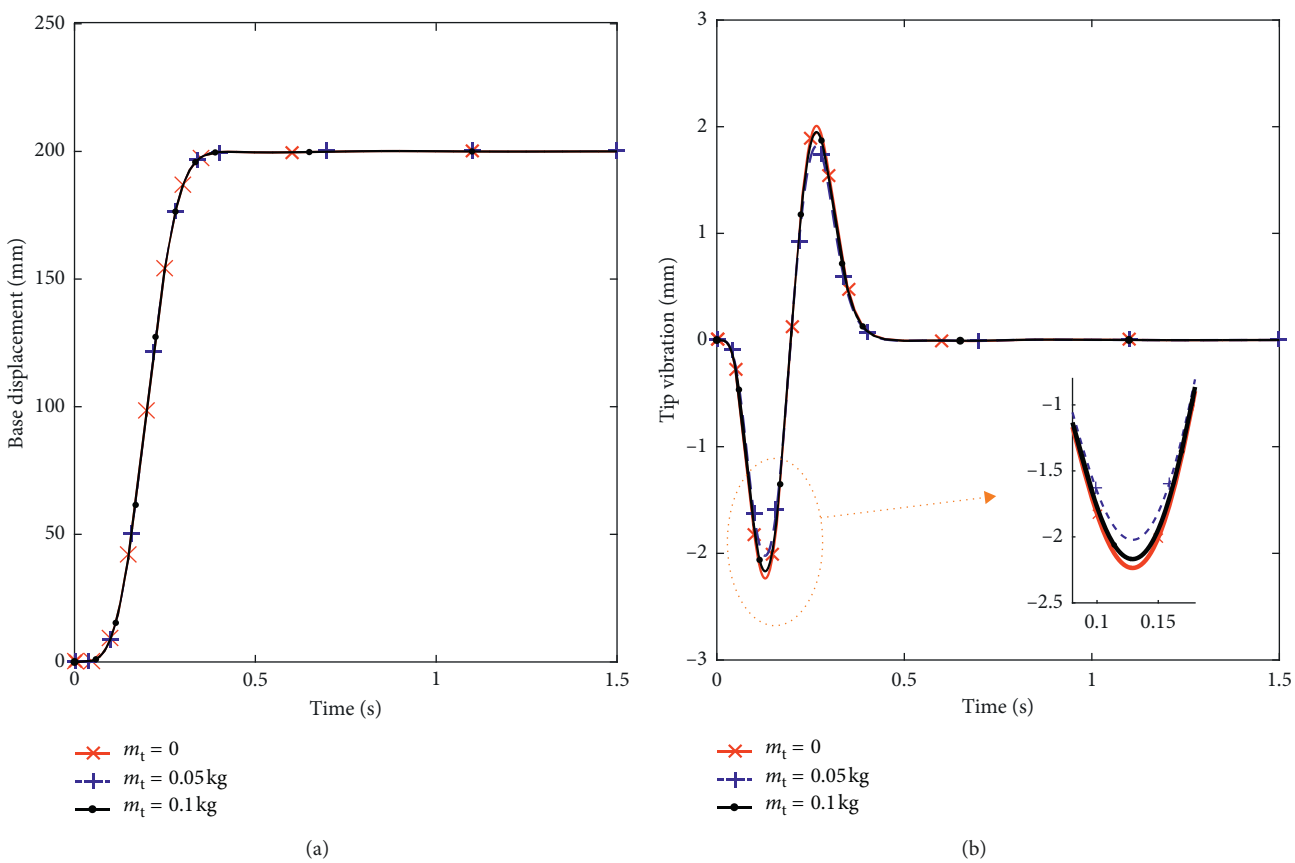

Figure 7: Control effect of the master-slave integrated controller under different terminal loads: (a) control effect of the base displacement; (b) control effect of the tip elastic vibration.

the two-mode vibration cascade shaper is improved and the contradictions of system rapidity and system overshoot for the SFIC can be effectively alleviated. The designed master-slave integrated controller can achieve the synchronous optimization of the system rapidity and accuracy.

5. Conclusions

With the time-lag filtering effect of the input shaper and the configuration capability of the state feedback for the closed-loop system poles considered, the SFIC and the two-mode vibration cascade shaper are combined to constitute the master-slave integrated controller for the elastic vibration of the TFMS for improving the robustness, the rapidity, and the accuracy of the system under variable load conditions. The following results are drawn:

(i) Based on the input shaping method and the cascade method, the designed two-mode vibration cascade shaper can effectively suppress the excitation of the motor output to the mode vibration of the flexible manipulator, but it is less robust when used alone.

(ii) Through comparing the control results of the master-slave integrated controller and the conventional input shapers with the SFIC, it is seen that the response speed of the two-mode vibration cascade shaper is better than that of the conventional input shapers and the time-lag effect of the conventional input shapers is effectively solved. Furthermore, the system response time and overshoot of the SFIC can be well taken into account to achieve a faster response speed without overshoot.

(iii) Under variable load conditions, the master-slave integrated controller can effectively control the elastic vibration of the TFMS and realize the complementary advantages and disadvantages of the SFIC and the two-mode vibration cascade shaper in the elastic vibration suppression of the TFMS.

Data Availability

The data used to support the findings of this study are available from the corresponding author upon request.

Conflicts of Interest

The authors declare that there are no conflicts of interest regarding the publication of this paper.

Acknowledgments

This research work was supported by the National Natural Science Foundation of China (No. 51805001), in part by the Anhui Provincial Natural Science Foundation (Nos.

1908085QE193 and 1808085QE137), and in part by the Research Starting Fund Project for Introduced Talents of Anhui Polytechnic University (No. 2018YQQ005).

References

[1] W. Jin, W. Lin, X. Yang, and H. Gao, "Reference-free path-walking method for ball grid array inspection in surface mounting machines," *IEEE Transactions on Industrial Electronics*, vol. 64, no. 8, pp. 6310–6318, 2017.

[2] J. Han and Y. Seo, "Mechanism to minimise the assembly time with feeder assignment for a multi-headed gantry and high-speed SMT machine," *International Journal of Production Research*, vol. 55, no. 10, pp. 2930–2949, 2017.

[3] D. Meng, Y. She, W. Xu, W. Lu, and B. Liang, "Dynamic modeling and vibration characteristics analysis of flexible-link and flexible-joint space manipulator," *Multibody System Dynamics*, vol. 43, no. 4, pp. 321–347, 2018.

[4] J. Wu, L. P. Wang, and L. W. Guan, "A study on the effect of structure parameters on the dynamic characteristics of a PRRRP parallel manipulator," *Nonlinear Dynamics*, vol. 74, no. 1-2, pp. 227–235, 2013.

[5] W. He and S. S. Ge, "Vibration control of a flexible beam with output constraint," *IEEE Transactions on Industrial Electronics*, vol. 62, no. 8, pp. 5023–5030, 2015.

[6] V. Feliu, E. Pereira, and I. M. Díaz, "Passivity-based control of single-link flexible manipulators using a linear strain feedback," *Mechanism and Machine Theory*, vol. 71, no. 1, pp. 191–208, 2014.

[7] M. Mahvash and P. E. Dupont, "Stiffness control of surgical continuum manipulators," *IEEE Transactions on Robotics*, vol. 27, no. 2, pp. 334–345, 2011.

[8] B. Zhou, B. Zi, and S. Qian, "Dynamics-based nonsingular interval model and luffing angular response field analysis of the DACS with narrowly bounded uncertainty," *Nonlinear Dynamics*, vol. 90, no. 4, pp. 1–28, 2017.

[9] M. Sadri, D. Younesian, and E. Esmailzadeh, "Nonlinear harmonic vibration and stability analysis of a cantilever beam carrying an intermediate lumped mass," *Nonlinear Dynamics*, vol. 84, no. 3, pp. 1667–1682, 2016.

[10] M. H. Korayem, M. Bamdad, H. Tourajizadeh et al., "Experimental results for the flexible joint cable-suspended manipulator of ICaSbot," *Robotica*, vol. 31, no. 6, pp. 887–904, 2013.

[11] B. Pratiher and S. Bhowmick, "Nonlinear dynamic analysis of a cartesian manipulator carrying an end effector placed at an intermediate position," *Nonlinear Dynamics*, vol. 69, no. 1-2, pp. 539–553, 2012.

[12] Y. S. Hamed, M. R. Alharthi, and H. K. Alkhathami, "Nonlinear vibration behavior and resonance of a cartesian manipulator system carrying an intermediate end effector," *Nonlinear Dynamics*, vol. 91, no. 3, pp. 1429–1442, 2018.

[13] B. Pratiher and S. K. Dwivedy, "Non-linear vibration of a single link viscoelastic cartesian manipulator," *International Journal of Non-Linear Mechanics*, vol. 43, no. 8, pp. 683–696, 2008.

[14] V. Spitsa, A. Alexandrovitz, and E. Zeheb, "Design of a robust state feedback controller for a STATCOM using a zero set concept," *IEEE Transactions on Power Delivery*, vol. 25, no. 1, pp. 456–467, 2010.

[15] W. He, S. S. Ge, Y. Li, E. Chew, and Y. S. Ng, "Neural network control of a rehabilitation robot by state and output feedback," *Journal of Intelligent & Robotic Systems*, vol. 80, no. 1, pp. 15–31, 2015.

[16] J. Deutscher and J. Gabriel, "Robust state feedback regulator design for general linear heterodirectional hyperbolic systems," *IEEE Transactions on Automatic Control*, vol. 63, no. 8, pp. 2620–2627, 2018.

[17] J. Song, L. Wang, G. Cai, and X. Qi, "Nonlinear fractional order proportion-integral-derivative active disturbance rejection control method design for hypersonic vehicle attitude control," *Acta Astronautica*, vol. 111, pp. 160–169, 2015.

[18] H. Guo, D. Wang, and J. Xu, "Research on a high-frequency response direct drive valve system based on voice coil motor," *IEEE Transactions on Power Electronics*, vol. 28, no. 5, pp. 2483–2492, 2013.

[19] L. Sun, W. Yin, M. Wang, and J. Liu, "Position control for flexible joint robot based on online gravity compensation with vibration suppression," *IEEE Transactions on Industrial Electronics*, vol. 65, no. 6, pp. 4840–4848, 2018.

[20] Q. Zhang, J. K. Mills, W. L. Cleghorn, J. Jin, and Z. Sun, "Dynamic model and input shaping control of a flexible link parallel manipulator considering the exact boundary conditions," *Robotica*, vol. 33, no. 6, pp. 1201–1230, 2015.

[21] J. Lin, C. S. Huang, and J. Chang, "A mechatronic kit with a control methodology for a modularized cable-suspended robot," *Journal of Vibration and Control*, vol. 22, no. 20, pp. 4211–4226, 2016.

[22] Z. Long, J. Zhang, Y. Liu, C. Han, Y. Li, and Z. Li, "Dynamics modeling and residual vibration control of a piezoelectric gripper during wire bonding," *IEEE Transactions on Components Packaging and Manufacturing Technology*, vol. 7, no. 12, pp. 2045–2056, 2017.

[23] Z.-C. Qiu, B. Wang, X.-M. Zhang, and J.-D. Han, "Direct adaptive fuzzy control of a translating piezoelectric flexible manipulator driven by a pneumatic rodless cylinder," *Mechanical Systems and Signal Processing*, vol. 36, no. 2, pp. 290–316, 2013.

[24] W. S. Rone and P. Ben-Tzvi, "Continuum robot dynamics utilizing the principle of virtual power," *IEEE Transactions on Robotics*, vol. 30, no. 1, pp. 275–287, 2014.

[25] X. Yao, X. Guo, Y. Feng, C. Yu, and C. Ma, "Dynamic analysis for planar beam with clearance joint," *Journal of Sound and Vibration*, vol. 339, pp. 324–341, 2015.

[26] B. Nayak, S. K. Dwivedy, and K. S. R. K. Murthy, "Dynamic analysis of magnetorheological elastomer-based sandwich beam with conductive skins under various boundary conditions," *Journal of Sound and Vibration*, vol. 330, no. 9, pp. 1837–1859, 2011.

[27] Y. Xing, E. Pedersen, and T. Moan, "An inertia-capacitance beam substructure formulation based on the bond graph method with application to rotating beams," *Journal of Sound and Vibration*, vol. 330, no. 21, pp. 5114–5130, 2011.

[28] H. N. Rahimi and M. Nazemizadeh, "Dynamic analysis and intelligent control techniques for flexible manipulators: a review," *Advanced Robotics*, vol. 28, no. 2, pp. 63–76, 2014.

[29] Z.-C. Qiu, "Adaptive nonlinear vibration control of a cartesian flexible manipulator driven by a ballscrew mechanism," *Mechanical Systems and Signal Processing*, vol. 30, pp. 248–266, 2012.

[30] E. Pereira, S. S. Aphale, V. Feliu, and S. O. R. Moheimani, "Integral resonant control for vibration damping and precise tip-positioning of a single-link flexible manipulator," *IEEE/ASME Transactions on Mechatronics*, vol. 16, no. 2, pp. 232–240, 2011.

[31] J. Y. Ju, W. Li, Y. Q. Wang, M. B. Fan, and X. F. Yang, "Two-time scale virtual sensor design for vibration observation of a translational flexible-link manipulator based on singular

perturbation and differential games," *Sensors*, vol. 16, no. 11, p. 1804, 2016.

[32] M. Biglar, H. R. Mirdamadi, and M. Danesh, "Optimal locations and orientations of piezoelectric transducers on cylindrical shell based on gramians of contributed and undesired Rayleigh-Ritz modes using genetic algorithm," *Journal of Sound and Vibration*, vol. 333, no. 5, pp. 1224–1244, 2014.

[33] J. Liu, Y. Li, Y. Zhang, Q. Gao, and B. Zuo, "Dynamics and control of a parallel mechanism for active vibration isolation in space station," *Nonlinear Dynamics*, vol. 76, no. 3, pp. 1737–1751, 2014.

[34] J. H. Chen, *The Research and Implementation of Input Shaping for Vibration Reduction*, Harbin Institute of Technology, Harbin, China, 2010, in Chinese.

[35] P. Melchior, A. Poty, and A. Oustaloup, "Motion control by ZV shaper synthesis extended for fractional systems and its application to CRONE control," *Nonlinear Dynamics*, vol. 38, no. 1–4, pp. 401–416, 2004.

[36] C.-W. Ha, D. Lee, K.-H. Rew, and K.-S. Kim, "An impulse-time perturbation approach for a symmetric extra-insensitive input shaper," *International Journal of Control, Automation and Systems*, vol. 16, no. 3, pp. 1239–1246, 2018.